Supplement of Earth Syst. Sci. Data, 18, 8407–8439, 2026
https://doi.org/10.5194/essd-18-8407-2026-supplement
© Author(s) 2026. CC BY 4.0 License.



Open Access Earth System Science Data

Supplement of

Global gridded air-sea oxygen flux inferred from a machine learning-based dissolved oxygen product

Yuming Jin et al.

Correspondence to: Yuming Jin (yumingjin@ucar.edu)

The copyright of individual parts of the supplement might differ from the article licence.

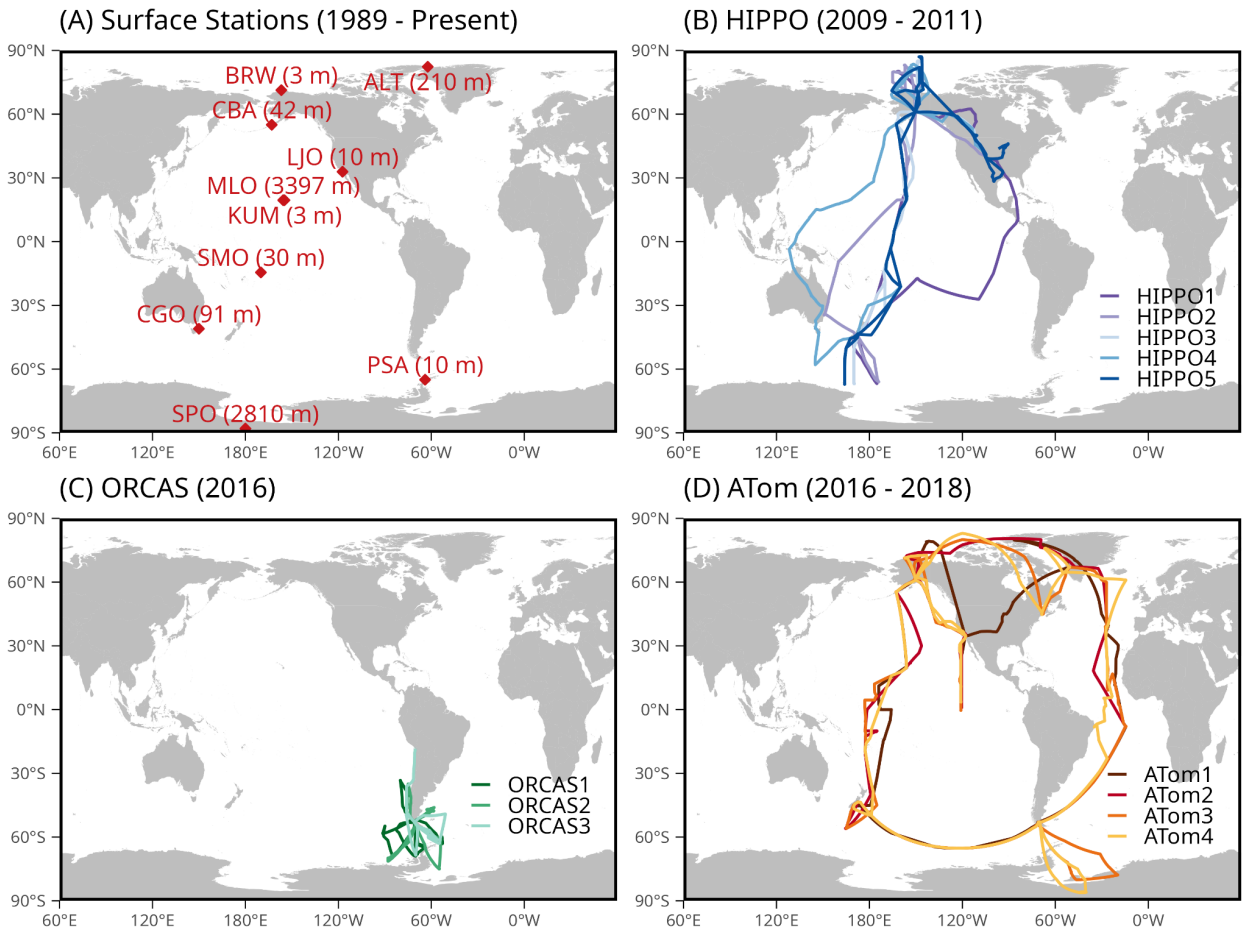


Fig. S1: Horizontal distribution of station and airborne measurements that provide atmospheric O_2 measurements used to evaluate the air-sea O_2 flux product. (A) Scripps O_2 program stations with station codes and inlet elevation in meters above sea level. (B) - (D) HIPPO, ORCAS, and ATom airborne campaign horizontal flight tracks.

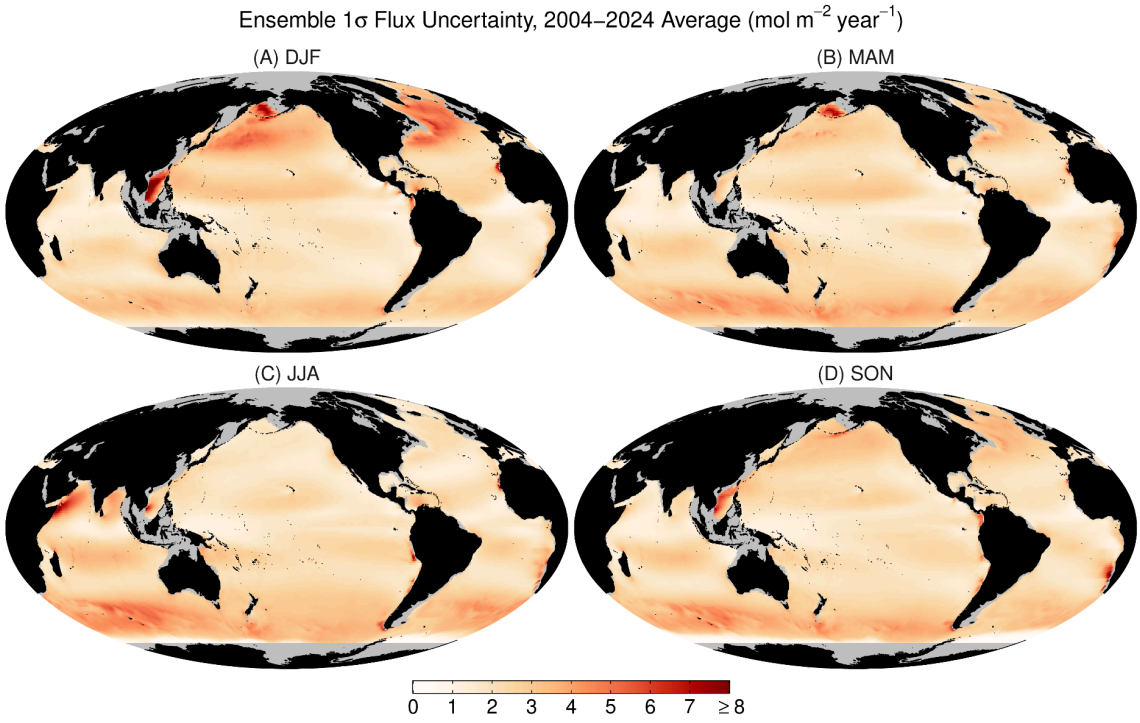


Fig. S2: Uncertainty in seasonal mean air-sea O_2 flux for (A) DJF, (B) MAM, (C) JJA, and (D) SON, based on GOBAI-O_2 v2.3, companion to Fig. 1. The uncertainty is computed as 1-σ across 9000 flux ensemble members.

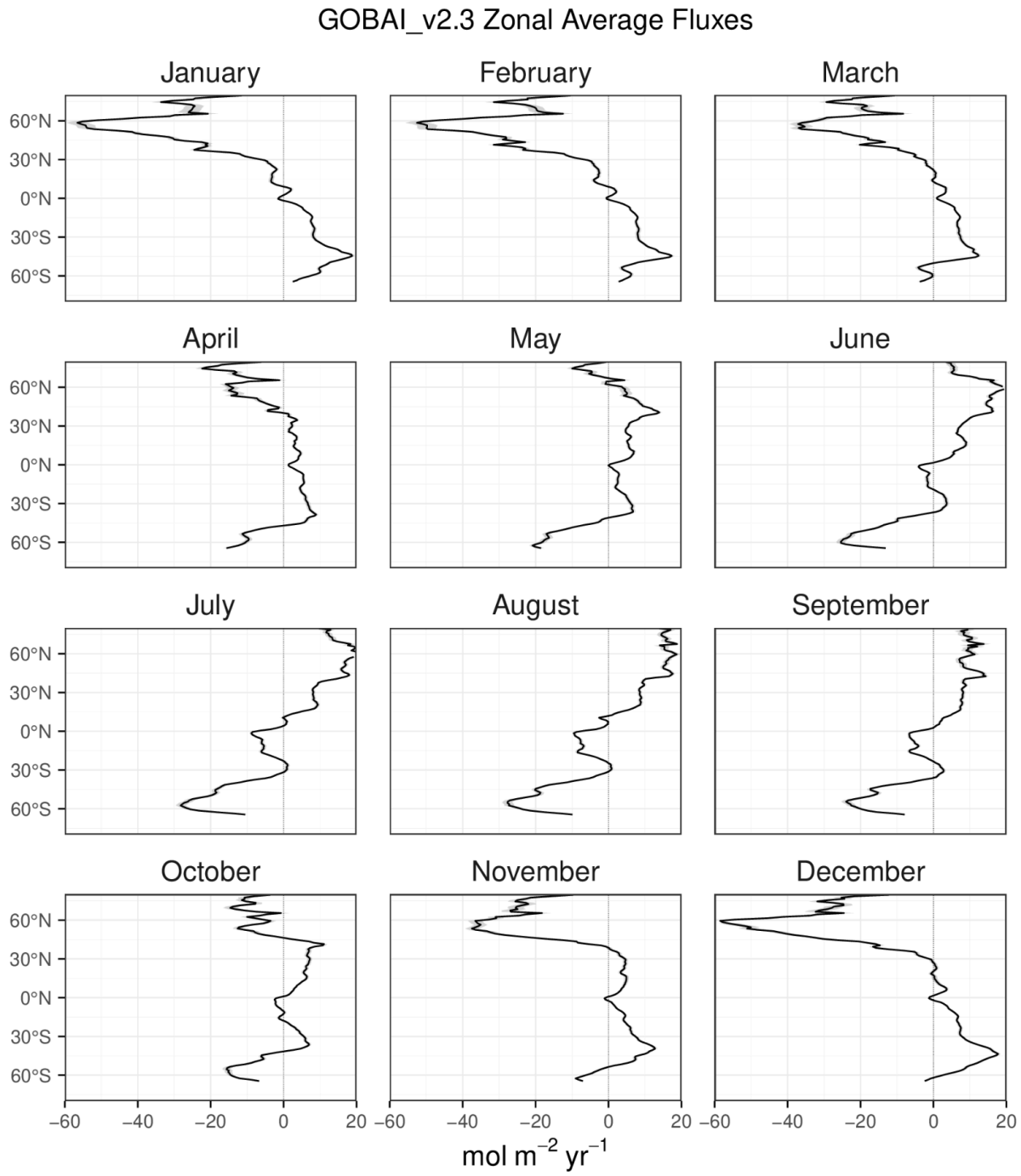


Fig. S3: Ensemble mean zonal mean flux (black lines) and 1σ uncertainty (gray shades) of each month, averaged from 2004 to 2024.

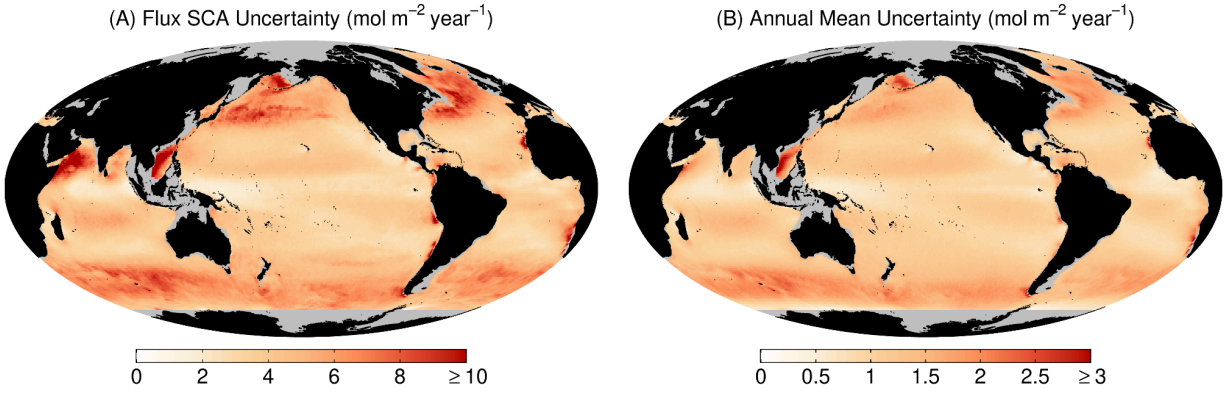


Fig. S4: Uncertainty in gridded air-sea O_2 flux (A) seasonal cycle amplitude (SCA), and (B) annual mean based on GOBAI-O_2 v2.3, companion to Fig. 3. The uncertainty is computed as 1-σ across 9000 flux ensemble members.

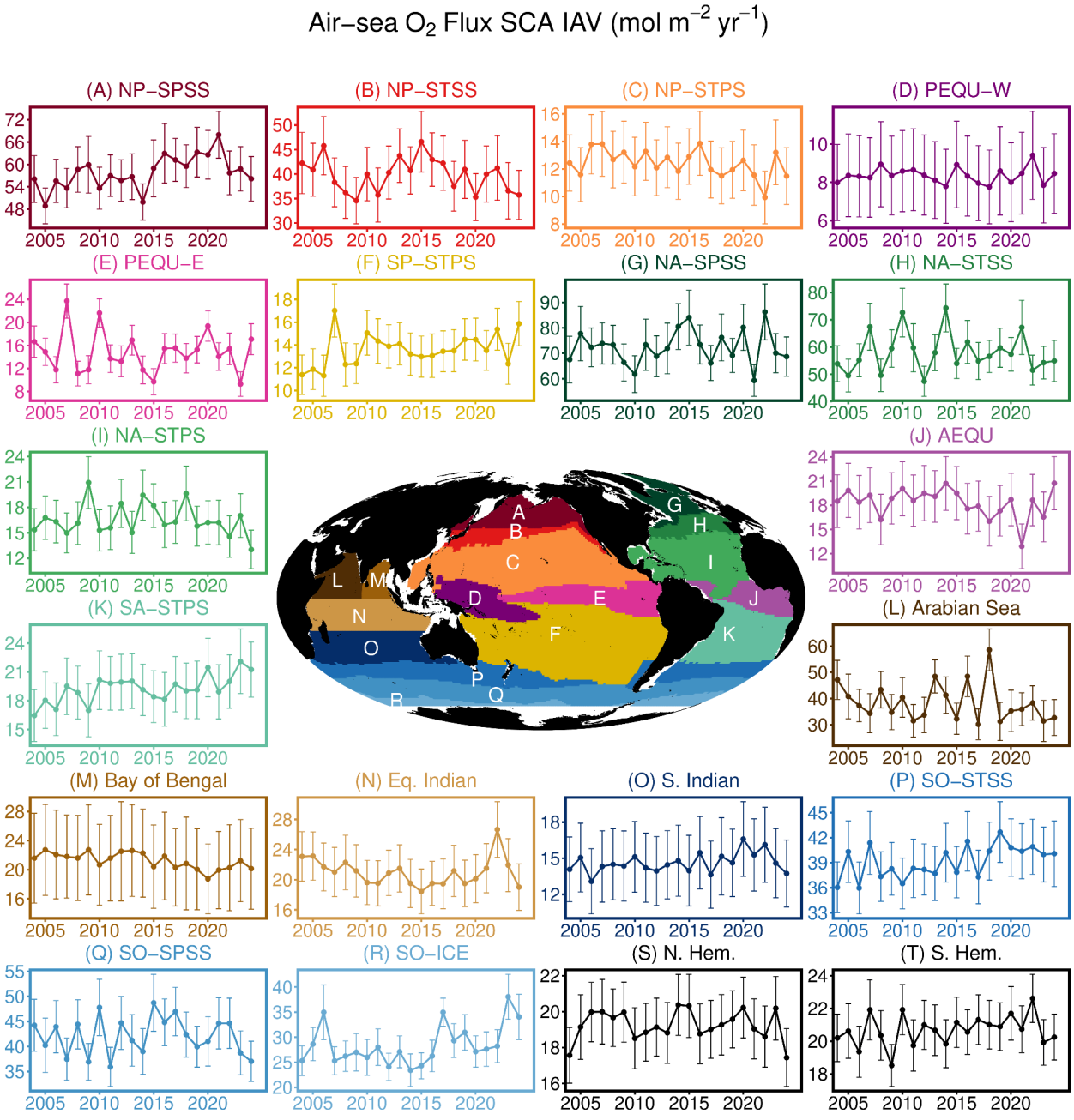


Fig. S5: Interannual variability of air-sea O_2 flux SCA, based on GOBAI-O_2 v2.3. SCA is calculated by first fitting a 2-harmonic function to the monthly fluxes of each region and each individual year, then taking the difference between the seasonal maximum and minimum. Error bars represent uncertainty calculated as standard deviation of all ensemble members. Panels are organized in the same order and colors as in Fig. 2. Panel titles and colors correspond to the region names and colors shown in the center map. Y-axis ranges vary across panels to optimize visualization of seasonal flux amplitude for each region.

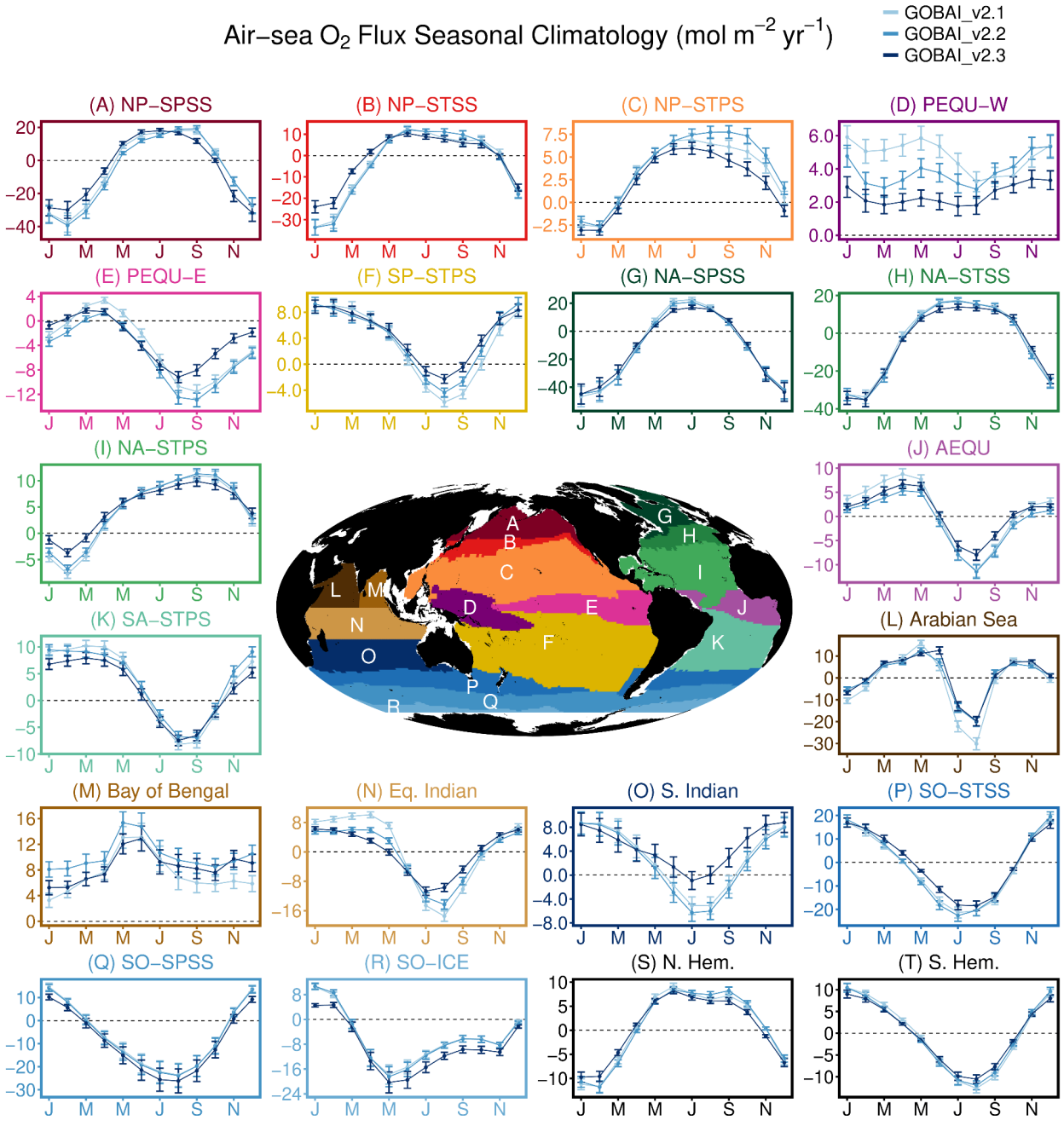


Fig. S6: Similar to Fig. 2, but showing comparison of regional climatological mean seasonal air-sea O_2 flux calculated using DO from three versions of GOBAI-O_2 (by color).

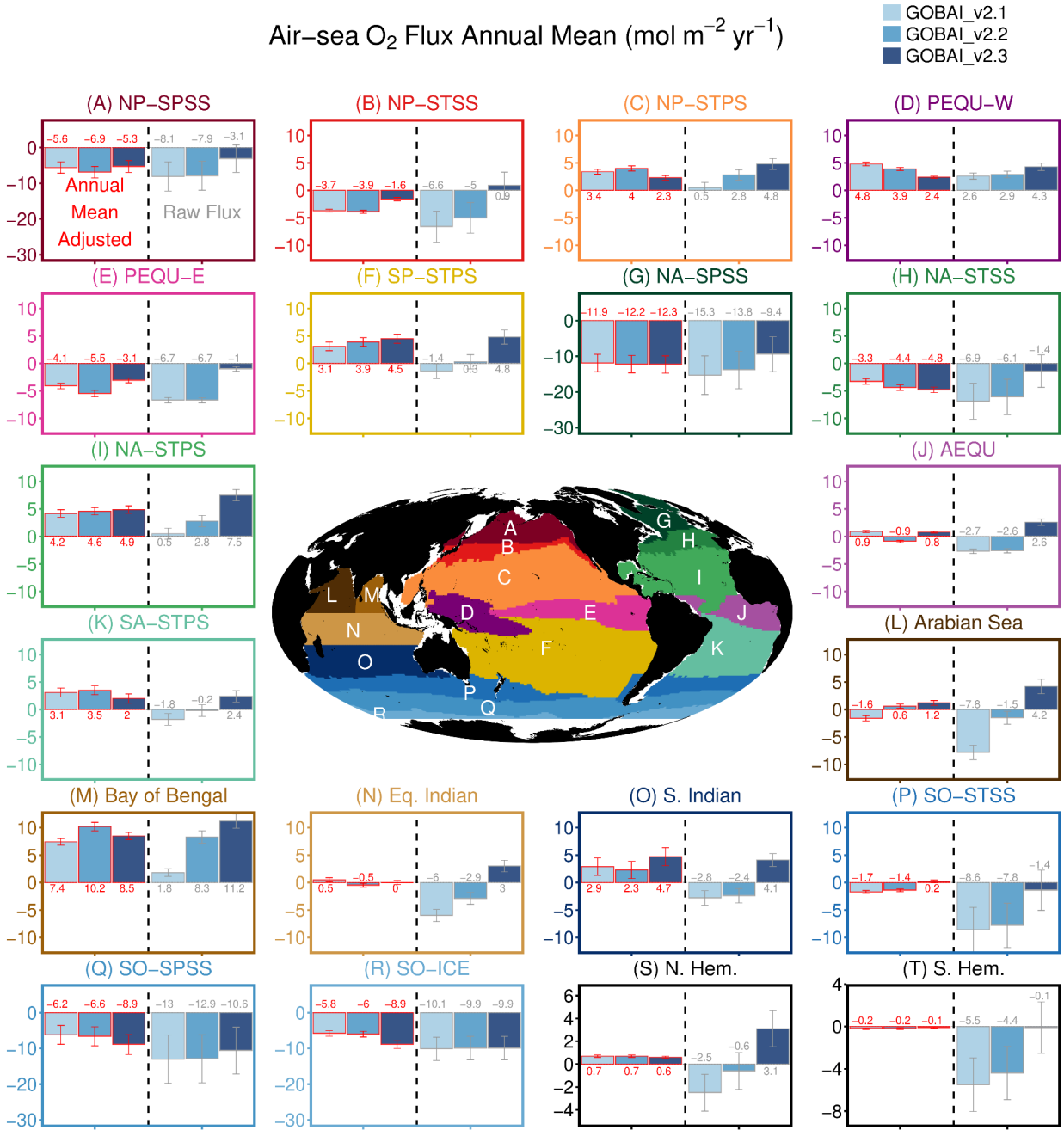


Fig. S7: Similar to Fig. 4, but showing comparison of regional annual mean air-sea O_2 flux resolved using DO from three versions of GOBAI-O_2 (by color).

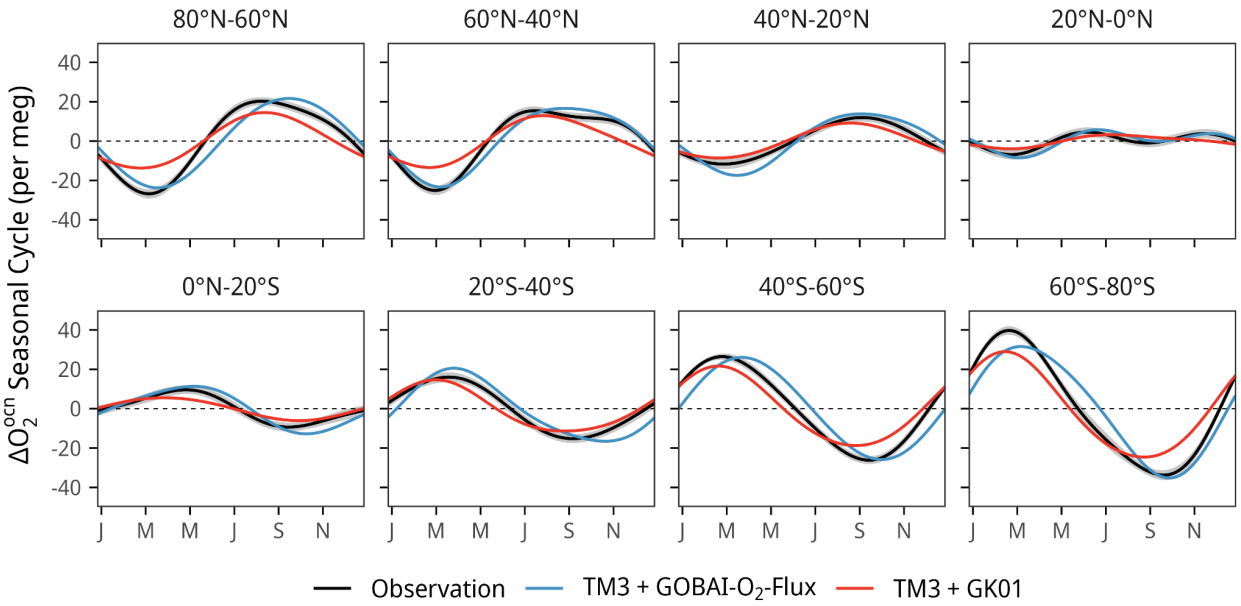


Fig. S8: Similar to Fig. 6, but comparing TM3 simulations of airborne tropospheric-average ΔO_2^{ocn} seasonal cycles using air-sea O_2 flux from GK01 (red, Garcia and Keeling, 2001) and our flux product (blue). The observed ΔO_2^{ocn} seasonal cycles are also shown in black.

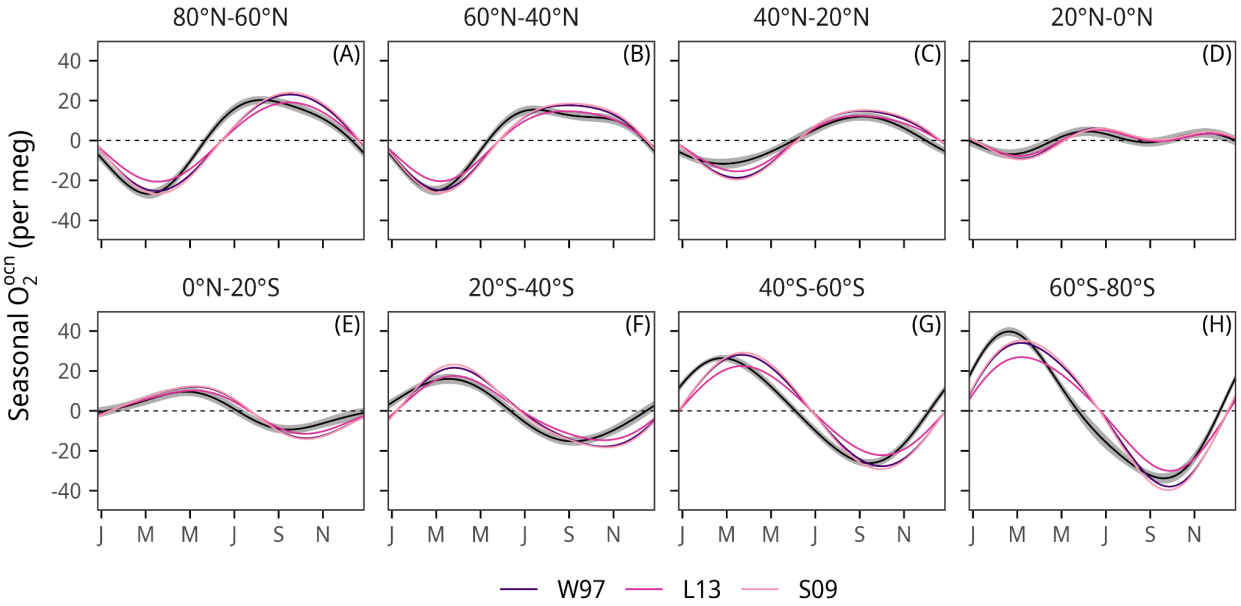


Fig. S9: Similar to Fig. 6, but comparing TM3 + GOBAI-O_2-Flux simulations of airborne tropospheric-average seasonal ΔO_2^{ocn} variations across eight latitude bands computed using different gas exchange parameterization schemes. The simulations are based on TM3 forward transport of ensemble mean fluxes calculated using each of the gas exchange schemes, and the CCMP wind product.

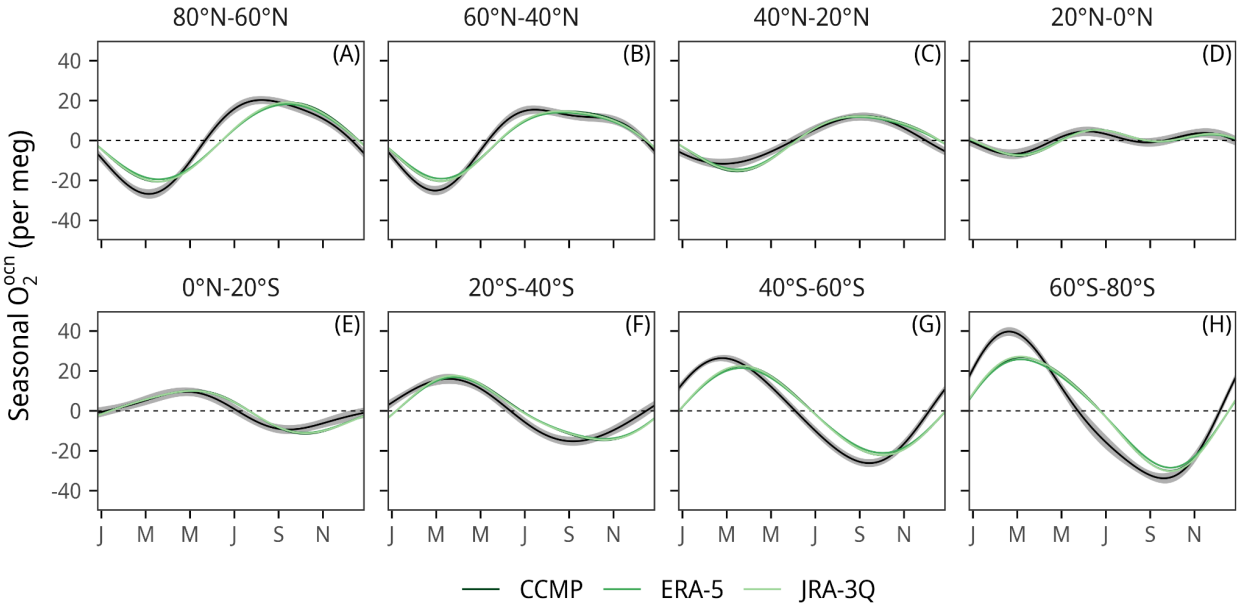


Fig. S10: Similar to Fig. 6, but comparing TM3 + GOBAI-O_2-Flux simulations of airborne tropospheric-average seasonal ΔO_2^{ocn} variations across eight latitude bands computed using different wind products. The simulations are based on TM3 forward transport of ensemble mean fluxes calculated using each of the wind products, and the L13 gas exchange parameterization scheme.

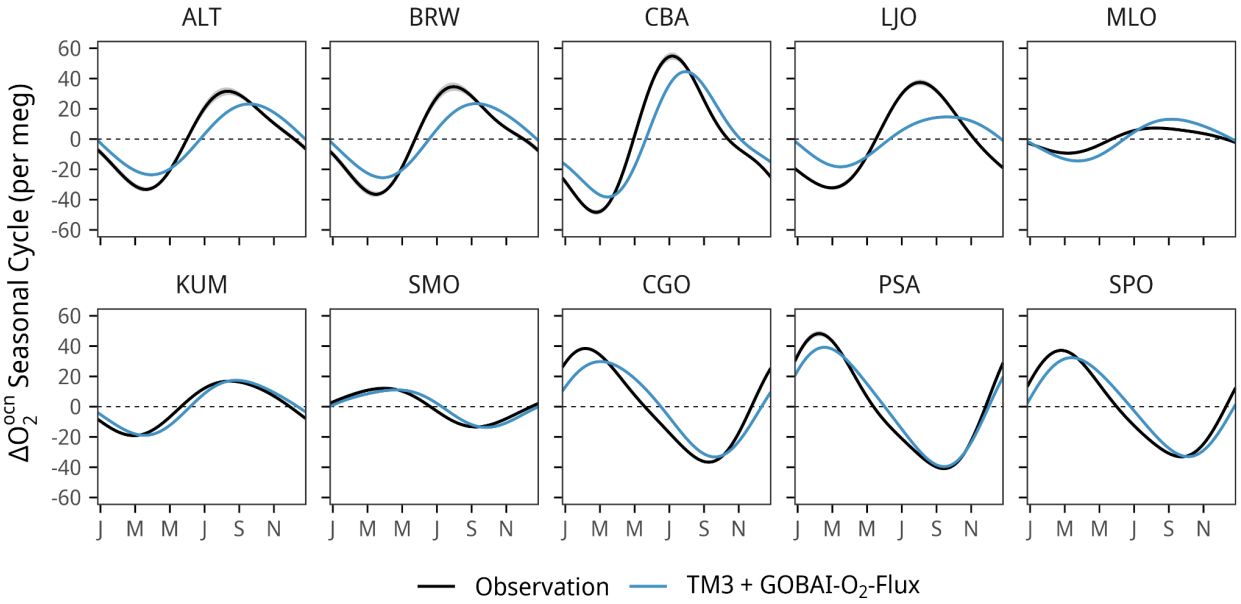


Fig. S11: Comparison of seasonal atmospheric ΔO_2^{ocn} between observations and TM3 + GOBAI-O_2-Flux simulations at 10 surface sampling sites along the Pacific basin. Panels are organized from northernmost to southernmost stations. Seasonal cycles are calculated following the same procedure as in Fig. 6 and averaged over 2005-2020, except for BRW, which is averaged over 2011-2020. Gray shading represents uncertainty of the observed seasonal cycle, combining measurement uncertainty and uncertainty in the atmospheric non-oceanic O_2 component corrections estimated from the ensemble of flux products and transport models (Appendix C).

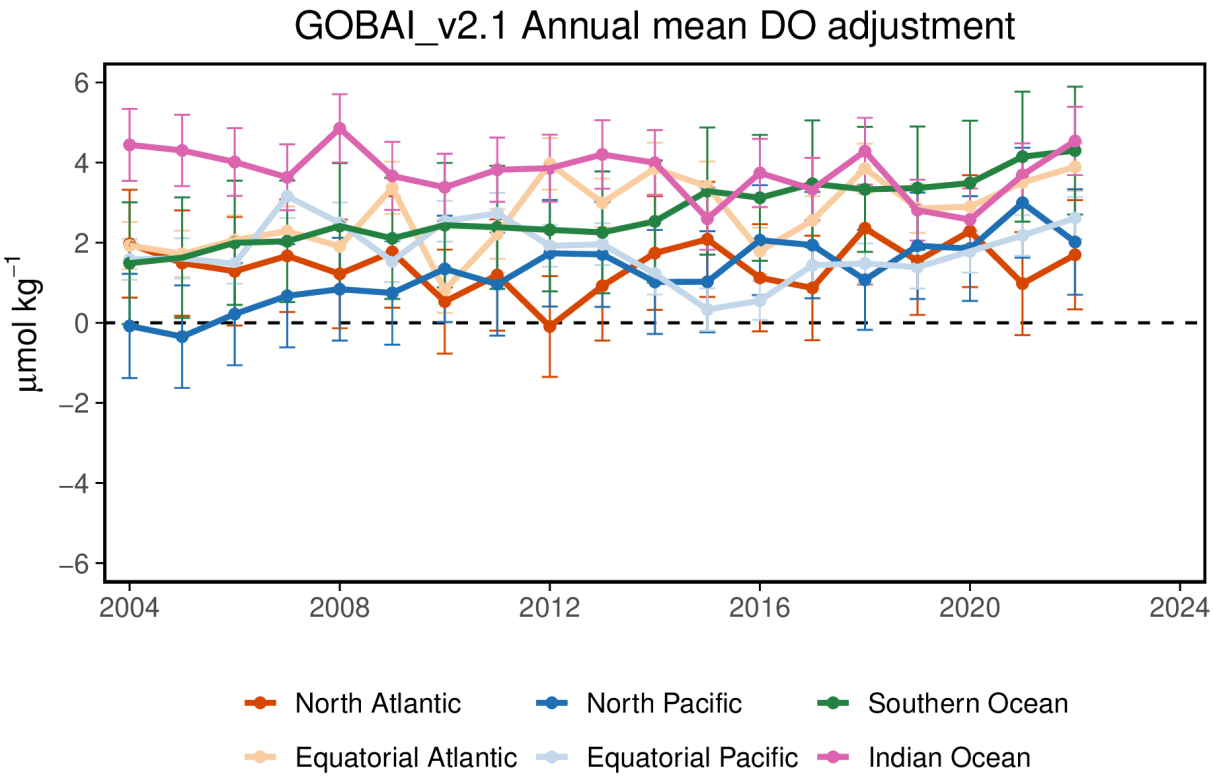


Fig. S12: Similar to Fig. B2, but showing DO adjustment for each of the six ocean regions (in Fig. B1), and each year for GOBAI-O_2 v2.1.

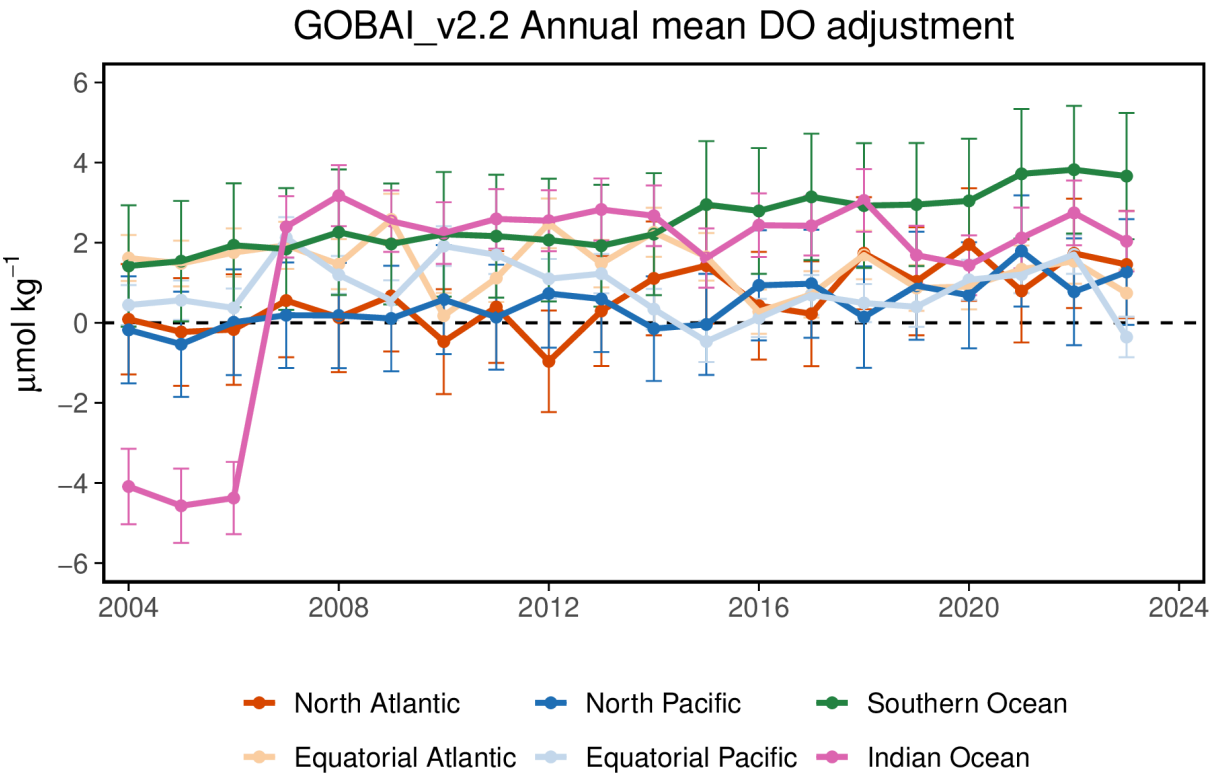
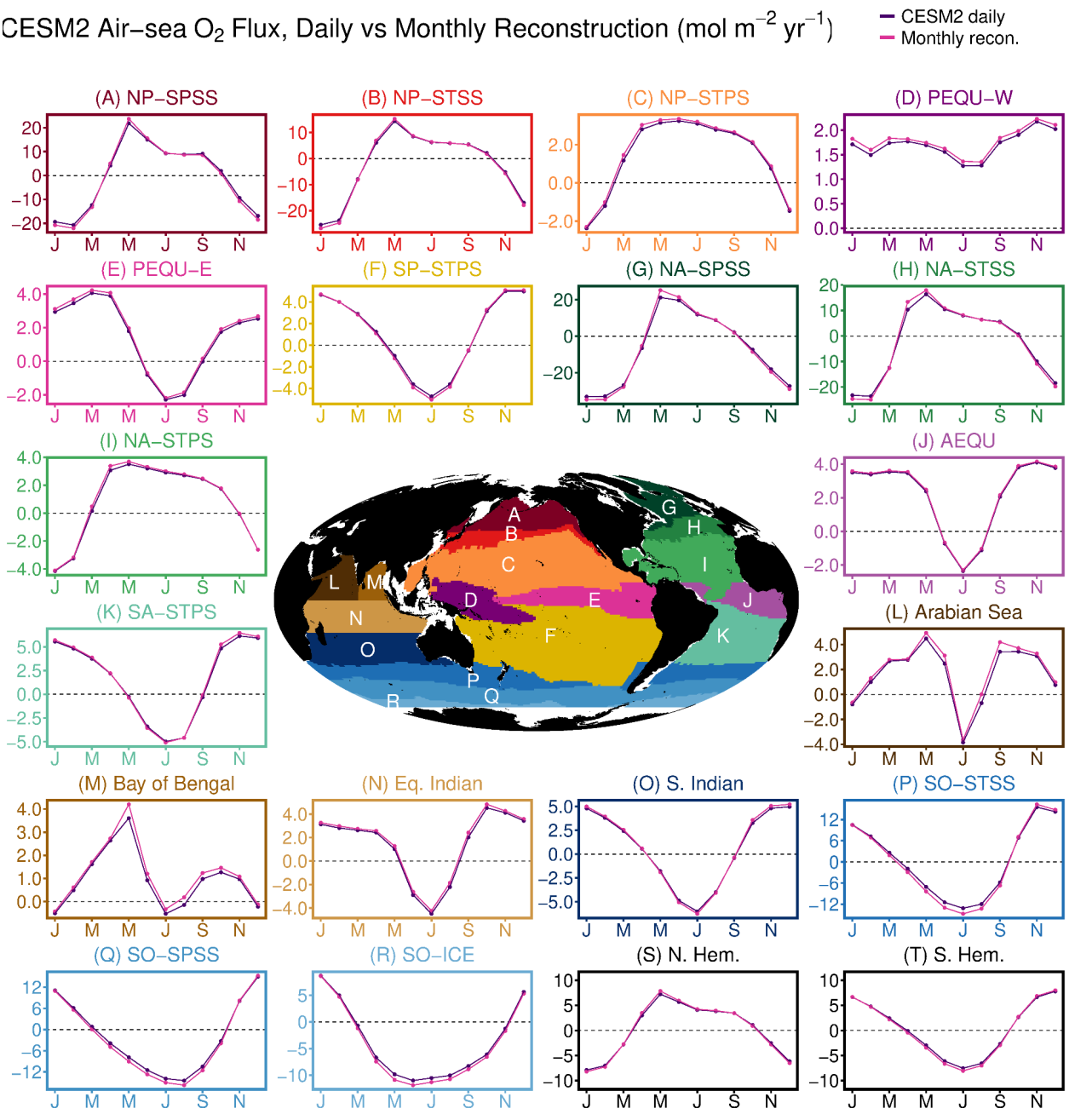


Fig. S13: Similar to Fig. B2, but showing DO adjustment for each of the six ocean regions (in Fig. B1), and each year for GOBAI-O_2 v2.2.



77

78 Fig. S14: Monthly climatology (2004-2020) of air-sea O_2 flux in the CESM2 FOSI simulation
79 for 18 RECCAP2 regions plus Northern and Southern Hemisphere averages, within the domain
80 of our flux product. The flux accumulated from daily model output (dark purple) is compared
81 with the flux reconstructed from monthly mean transfer velocity, DO anomaly, and ice fraction
82 (pink). The difference between the two curves isolates the effect of neglecting sub-monthly
83 covariance between the gas transfer velocity and the DO anomaly (Section 4.1). The center map
84 shows the region boundaries as in Fig. 2. Positive values indicate outgassing.

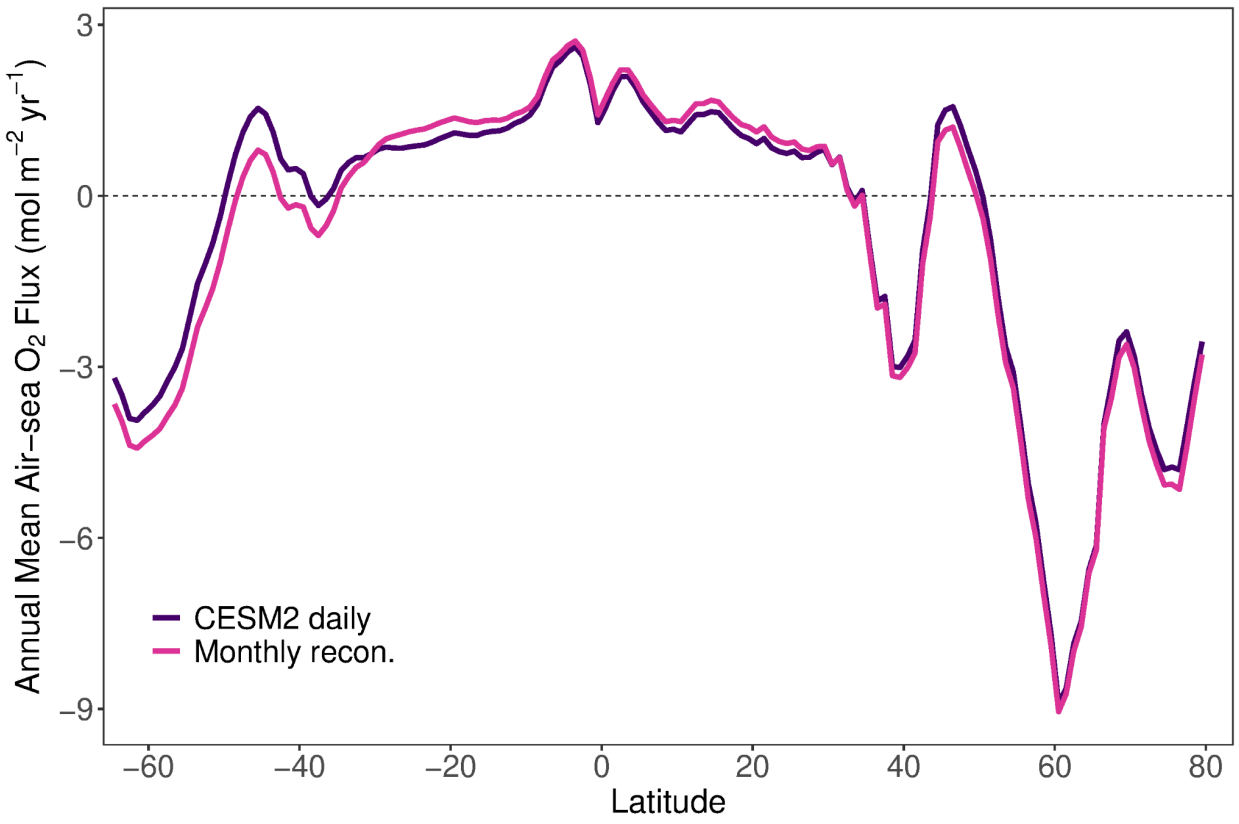


Fig. S15: Zonal annual mean air-sea O_2 flux (2004-2020) in the CESM2 FOSI simulation, computed from daily model output (dark purple) and from the monthly mean reconstruction (pink), following the same procedure as Fig. S14. Neglecting sub-monthly covariance overestimates the ingassing between 45°S and 65°S and overestimates the outgassing near the equator, increasing the meridional gradient of the annual mean flux.

References

Garcia, H. E. and Keeling, R. F.: On the global oxygen anomaly and air-sea flux, J. Geophys. Res. Oceans, 106, 31155–31166, https://doi.org/10.1029/1999JC000200, 2001.